Ammonium removal and recovery from municipal wastewater by ion exchange using a metakaolin K-based geopolymer

Highlights

- Ammonium recovery from real municipal wastewater in a continuous flow plant process
- Ammonium adsorption test on saline wastewater characterized by cations competition
- Geopolymer granules showed high ammonium selectivity and adsorption capacity
- Geopolymer granules did not deteriorate after adsorption/regeneration cycles
- Geopolymer allows to obtain a Na-free desorbed product potentially good as fertilizer

Ammonium removal and recovery from municipal wastewater by ion exchange using a metakaolin K-based geopolymer

Valentina Medri[a]*, Elettra Papa[a], Elena Landi[a], Carla Maggetti[b] Davide Pinelli[b], Dario Frascari[b]
[a] National Research Council of Italy, Institute of Science and Technology for Ceramics (CNR-ISTEC), Via Granarolo 64, 48018 Faenza, RA, Italy
[b] Department of Civil, Chemical, Environmental and Materials Engineering (DICAM), Alma Mater Studiorum – University of Bologna, via Terracini 28, 40131 Bologna, Italy

***Corresponding Author:**
Valentina Medri
Tel: +39 0546 699751
Fax: +39 0546 699799
e-mail: valentina.medri@istec.cnr.it

Abstract:
Among the available technologies for ammonium removal from wastewater, ion exchange represents one of the most promising ones in the perspective to recover ammonium and produce a fertilizing product. However, the vast majority of previous studies on ammonium ion exchange did not evaluate the process robustness under real operational conditions nor optimized the desorption step. In this paper, tests of ammonium removal and recovery were conducted on a metakaolin K-based geopolymer, compared with a high-performing Italian natural zeolite in K-form. Real municipal and saline wastewater was treated in a continuous flow pilot plant equipped with a 60-cm adsorption bed (bed volume 203 mL, sorbent mass 145-173 g, empty bed contact time 10 minutes). Geopolymer granules showed higher performances in terms of selectivity towards ammonium, operating capacity (8.5 mg_N g^{-1} dry adsorbent at an inlet concentration of 40 mg_N L^{-1}), bed volumes of wastewater treated at the selected breakpoint (149). Geopolymer resulted to be a cost-effective adsorbent for wastewater treatment capable to adsorb cations by ion exchange, allowing a fractionated desorption procedure that led to recover ammonium in a solution composed mainly by NH_4NO_3 (37%$_{wt}$) and KNO_3 (56%$_{wt}$), potentially usable as fertilizer. The geopolymer robustness was assessed after repeated adsorption/regeneration cycles showing that the geopolymer mechanical and morphological properties did not deteriorate. The results make the tested geopolymer a very promising material for the optimization and scale-up of the ammonium recovery process in a circular economy perspective.

Keywords: ion exchange, geopolymer, natural zeolite, ammonium recovery, nutrient recovery, wastewater treatment.

1. Introduction

One of the major concerns deriving from environmental pollution is the contamination of water bodies. Among wastewater contaminants, that include bacteria, heavy metals and dyes, the excessive presence of nitrogen in water, such as ammonium (NH_4^+), primarily originated from municipal sewage, fertiliser and agricultural wastes (Wang and Peng, 2010), accelerates the eutrophication of lakes and rivers (Tan et al., 2020; Guida et al., 2020). For this reason, the Water Framework Directive 2000/60/EC and Council Directive 91/271/EEC regulated collection, treatment and discharge of urban wastewater, to protect the environment from eutrophication.
Concerning ammonium removal from municipal wastewaters (MWW), the current typical technique is the biological nitrification/denitrification process that converts ammonium into gaseous N_2. However, this process has a substantial energy consumption and does not allow any N recovery. Several technologies allow the removal and recovery of NH_4^+ from WW in a circular economy perspective (Beckinghausen et al., 2020). Among them, adsorption and ion-exchange (IE) are very promising technologies for N recovery when ammonium is at medium/low concentration, as in

MWW. Thus, ion exchange treatments are becoming nowadays more and more interesting than conventional biological treatments (Carrera et al., 2003), because they are based on easy-to-use and cost-effective solid adsorbents with lower environmental impact (lower CO_2 emission) (Guida et al., 2020; Huang et al., 2020). A key component of the process is the sorbent that should have a high capacity and selectivity. Naturally occurring zeolites, in particular clinoptilolite in Na-form, are especially attractive for NH_4^+ adsorption (Guida et al., 2020; Jha and Hayashi, 2009). In fact, natural zeolites are microporous and low-cost adsorbents with Na^+, K^+, Mg^{2+} and Ca^{2+} exchangeable cations, that make them particularly suitable for wastewater treatment (Tasić at al., 2019).

Furthermore, the Si/Al ratio of zeolites influences both adsorption and ion exchange capacity. Clinoptilolite, having a high molar Si/Al ratio (4.58), possesses a high adsorption capacity for NH_4^+ due to the presence of six- to twelve-membered ring channels that help the entry of cations also when hydrated (Chen et al., 2018). However, a low Si/Al ratio increases the number of exchangeable cations since Al atoms add negative charges in the framework. For this reason, natural zeolites such as merlinoite or chabazite, with Si/Al molar ratios between 2 and 3, have high NH_4^+ exchange capacities (Chen et al., 2018).

Despite the cheapness of natural zeolites is indisputable, they are less performant in ammonium exchange capacity than the more expensive synthetic ones. This is mainly due to the octahedral coordination of Al^{3+} occurring in natural zeolites instead of the tetrahedral coordination in synthetic zeolites, even though thermal and chemical treatments can be performed to improve the selectivity and ion exchange capacity of natural zeolites (Thornton, 2007; Guida et al., 2020).

In this scenario, geopolymer technology is gaining interest in research and development, because it is based on versatile mesoporous materials with many potential applications in water and wastewater treatment (Luukkonen et al., 2019; El-Eswed, 2019), including adsorbents/ion-exchangers, membranes and filters, photocatalysts, antimicrobials, buffers and carriers for bioreactors (Luukkonen et al., 2019; El-Eswed, 2019; Asim et al., 2019; Rasaki et al., 2019; Siyala et al., 2018; Novais et al., 2017). Geopolymers can boast high mechanical performance with an easy shaping and reproducibility (Medri et al., 2020a) even on a large scale, with a production process less expensive than those required for synthetic zeolites. In fact, geopolymers are synthetic alkali aluminosilicates produced by the reaction of an aluminosilicate powder with an alkali aqueous solution at a temperature below 100°C. Although geopolymers are amorphous due to the short-range ordering of their network, Al is in tetrahedral coordination in eight-membered or larger aluminosilicate rings as in synthetic zeolites (Bortnovsky et al., 2008), depending on the Si/Al ratio which can be easily modified in the staring formulation (Davidovits, 2008). Furthermore, mesoporous geopolymers can be shaped with interconnected micro-meso-macro-ultramacro porosities as monoliths (Medri et al., 2013; Papa et al., 2015), beads (Ge et al., 2015; Medri et al., 2020b) and components fabricated by 3D printing (Franchin et al., 2020), enabling a fast mass transport and diffusion of cations towards the internal porosity.

As zeolites, geopolymers preferentially adsorb cations by ion-exchange. Bibliographic data regarding geopolymer adsorption performances are affected by test conditions and protocols (stationary or in flux, cations starting concentrations, pH, etc.), geopolymer stoichiometry (Si/Al ratio, charge balancing cation) and shape (granules size, macro-porosity, etc.), resulting in a wide range of results. For example, regarding ammonium Luukkonen et al., 2018 reported that using a powdered metakaolin-based geopolymer with Si/Al and Na/Al ratios around 1.4 and 0.4 respectively, the maximum ammonium exchange capacities were 31.79, 28.77, and 17.75 $mg_N\ g^{-1}$ in synthetic, screened, and pre-sedimented municipal wastewater, estimated using the asymptotic values of the relative isotherms. However, using millimetric granulated geopolymer in a wastewater treatment plant the exchange capacity decreases below 4 mg g^{-1}. Sanguanpak et al., 2021, reported that macro-porous metakaolin-based geopolymer granules, with Na as charge balancing cation, reached a removal efficiency of 84% for piggery wastewater at a NH_4^+ starting concentration of 75 mg L^{-1}. Franchin et al., 2020, reported that 3D-printed metakaolin-based geopolymers with Si/Al =1.9 and

Na/Al = 1.0 have ion-exchange capacity larger than 2.6 mg g^{-1} and removal efficiency over 80% in a NH_4^+ model solution.
NH_4^+ removal efficiency is generally higher using Na^+ as adsorbent charge balancing cation than K^+ (Luukkonen et al., 2017). Since Na^+ has lower hydration energy, because of the smaller atomic radius, it is fixed in a less stable way to the ion exchanger. However, in this work, in view of a potential reuse of the recovered ammonium as a fertilizer, potassium was selected as a regenerating agent, being Na^+ harmful for plants and soil.
The main goal of this work was to compare a metakaolin-based geopolymer, having a Si/Al ratio equal to 2 and K^+ as exchangeable cation (Bell et al., 2009; Landi et al., 2013), with an Italian natural zeolite activated in K^+ form and containing chabazite and phillipsite with a Si/Al ratio close to 2 (Shoumkova, 2011), in terms of ammonium retention/recovery performances and granules characterization. Recently, Niu et al (2022) reported that a metakaolin-based geopolymer with the same stoichiometry studied in this work had a negative zeta potential regardless of pH, therefore the surface was permanently charged allowing adsorption of cations through electrostatic interactions. The tests were conducted following a procedure that integrates batch isotherm tests – often used in the literature to compare materials for adsorption processes - with continuous-flow adsorption/desorption tests that allow to assess key parameters, such as the adsorbent operating capacity at the selected breakpoint and the process robustness (Pinelli et al., 2022). The tests were conducted with a saline wastewater containing other competing cations in addition to NH_4^+. An in-depth characterization of the fresh and used geopolymer granules was performed, in order to assess the entity of material deterioration after adsorption/desorption cycles.
The main novelties of this work are: i) the development of a process of ammonium recovery with geopolymers from real municipal wastewater (MWW) in a continuous flow pilot plant equipped with a 60-cm, 0.20 L adsorption bed; ii) the use in the tests of a saline MWW due to the presence of a local hotspot of seawater intrusion, characterized by a strong competition between ammonium and other cations; iii) the development of a fractionated desorption process aimed at obtaining a nearly Na-free product potentially usable as fertilizer. To the best of the authors' knowledge, none of the previous studies on ammonium recovery from MWW, with either zeolites or geopolymers, have included the optimization of the desorption step in order to obtain a fertilizing product.

2. Materials and Methods

2.1 Materials

Metakaolin K-based geopolymer coded as G13, with theoretical molar ratios Si/Al = 2 and K/Al = 1 was synthetized as reported in (Papa et al., 2022). The G13 slurry was placed in a plastic mould and cured in a heater at 80°C for 24 h in a closed vessel and then for further 24h in an open vessel.
A zeolite-bearing rock from pyroclastic deposits of volcanic origin (Apostolico & Tanagro s.n.c., Naples, Italy), containing sanidine (K-feldspar), biotite (mica), pyroxene and 50 to 80%$_{wt}$ of chabazite and phillipsite, was used as natural zeolite adsorbent.
G13 and natural zeolite granules were prepared by crushing and sieving the materials in the range of 355-710 µm, and were used for the characterizations and the ammonium adsorption tests.

2.2 Adsorption/desorption tests

2.2.1 Wastewater and synthetic solution composition

Isotherms and continuous flow tests were conducted with an actual high-salinity treated municipal wastewater (TMWW), namely the effluent of a pilot-scale anaerobic membrane bioreactor, placed in side-stream configuration after an Up-flow Anaerobic Sludge Blanket reactor that treats the saline MWW of Falconara Marittima (Italy) (Foglia et al., 2020). This MWW is particularly challenging for an ion exchange process as it is saline due to the presence of a local hotspot of seawater intrusion.
The saline TMWW was spiked with NH_4Cl to obtain 40 mg_N L^{-1}, corresponding to the average ammonium content of the effluent of a MWW treatment plant in which nitrogen removal is not

performed. The detailed composition of the TMWW is reported in Table 1. The Falconara groundwater is subject to a significant seawater intrusion, thus the studied TMWW is characterized by high concentrations of Na^+ (214±7 mg L^{-1}), Cl^- (311±3 mg L^{-1}), K^+ (24±3 mg L^{-1}), Mg^{2+} (32±1 mg L^{-1}) and Ca^{2+} (97±9 mg L^{-1}).

2.2.2 CEC assessment

Cation exchange capacity (CEC) was assessed by using a 5-step experimental method based on the common practice of commercial cation exchangers characterization (Rohm and Hass, 2005). The test was carried out in a laboratory column with an inner diameter of 13 mm, packed with a 100 mm adsorption bed of the sorbent to be analyzed. In the first step, the bed was conditioned to K^+ form eluting 12 bed volumes (BVs) of a 1 M solution of KCl with a 4 BV/h flow rate, corresponding to the typical range applied in the desorption/regeneration step at laboratory scale (Rohm and Hass, 2005). In the second step, 4 BVs of deionized water were eluted to remove the K^+ cations from the liquid of the bed. In the third step, K^+ was displaced by NH_4^+. In the fourth step, a second wash was performed with 4 BVs of deionized water. Finally, in the fifth step, 12 BVs of a 12M solution of KCl were eluted to displace the previously adsorbed NH_4^+. The relatively high concentration of the regenerant was chosen to reduce the duration of the desorption phase.
The CEC was assessed by analyzing K^+ and NH_4^+ contents in the eluted solutions generated by steps 3 and 5. Thus, two values were obtained by dividing the equivalents of displaced cations by the mass of sorbent loaded in the column:

$$CEC_K = V_{L,step\ 3} \cdot C_K / m_{dry\ sorbent} \quad (1a)$$

$$CEC_N = V_{L,step\ 5} \cdot C_N / m_{dry\ sorbent} \quad (1b)$$

where $V_{L,step\ 3}$ and $V_{L,step\ 5}$ indicate the total volume of effluent collected from the column during step 3 (K^+ displacement with NH_4^+) and step 5 (NH_4^+ displacement with K^+), whereas C_K and C_N indicate the concentrations of K^+ and N- NH_4^+ in the two collected effluents. The mean of these two values was assumed as the best estimate of CEC for the tested sorbent, in order to obtain a reliable CEC estimate and to reduce the CEC confidence interval. The number of BVs used to completely exchange the cations in the sorbent was calculated as five times the one that is necessary to feed the equivalents corresponding to the expected cation exchange capacity (Rohm and Hass, 2005). The actual saturation of the bed was verified by monitoring the displaced cation until it disappeared from the outlet stream at the end of steps 3 and 5. The resulting CEC values were compared with the data obtained from the isotherm batch tests (see section 3.1.1 Isotherm tests).

2.2.3 Adsorption isotherm tests

Isotherm tests were performed with the actual high-salinity TMWW. A nitrogen concentration range up to 600 mg_N L^{-1} was tested at room temperature (20-22°C), in glass bottles containing 100 mL of spiked TMWW and 2 g L^{-1} of dry adsorbent which were agitated for 7 h in a rotatory shaker (200 rpm) to reach equilibrium. The time needed to reach equilibrium was defined according to the results of preliminary kinetic tests (data not shown). The N concentration at equilibrium in the solid phase, $C_{S,eq}$, was expressed as mg_N per gram of dry adsorbent and determined according to Eq. (2):

$$C_{S,eq} = \frac{(C_{L,0} - C_{L,eq}) \cdot V_L}{m_S} \quad (2)$$

where m_S is the mass of dry adsorbent, $C_{L,0}$ and C_L are the initial and final N concentrations in the liquid and V_L is the liquid volume.
Each test was performed in triplicates and the 95% confidence intervals associated to $C_{S,eq}$ were calculated from the standard deviation of the mean values. The experimental data were interpolated by means of the Langmuir model. The model parameters were estimated by non-linear least squares regression of the calculated N solid phase concentrations to the corresponding experimental values. More details about apparatuses and procedures can be found in Pinelli et al., 2022.

2.2.4 Continuous flow breakthrough tests

The continuous flow adsorption/desorption tests (breakthrough tests, BT) were conducted with N-spiked TMWW in a PVC column with a total volume of 0.436 L, a total height of 1.26 m and an inner diameter of 21 mm.
The final adsorbent bed height was 60 cm, the minimum value commonly used in industrial applications. After column packing, the natural zeolite adsorbent was activated in K^+ form through the elution of 10 bed volumes (BVs) of a 100 g L^{-1} KCl solution, while G13 was directly produced in K^+ form. Before conducting the breakthrough tests, the fluid dynamic behaviour of the adsorption bed was studied by means of conventional frontal analysis tests conducted with a KCl solution as the tracer. Adsorption was performed at a 10-minute empty bed contact time (EBCT, defined as the volume of adsorption bed over the volumetric flow rate), a typical value commonly used in ion exchange tests (Hedström, 2001). The BT was carried out at a constant column temperature of 22°C; pressure drop and flow rate were measured hourly. Outlet samples were collected and analysed every 30 minutes, inlet samples were collected every 3 h. Cation outlet concentrations were normalized by the average inlet concentration. The adsorption performances were quantified at a breakpoint (BP) corresponding to an outlet concentration of 4 mg_N L^{-1}. Three main parameters were used to describe the performance at the BP: i) the number of BVs needed to reach the BP, defined as (TMWW volume treated at the BP)/(adsorbent BV), ii) the adsorbent operating capacity, defined as (N mass adsorbed at the BP)/(adsorbent dry mass), and iii) the NH_4^+ adsorption yield (Y_{ads}), a dimensionless parameter defined as (N mass adsorbed at BP)/(N mass fed at BP). The N mass adsorbed at the BP ($m_{N,sorbed,BP}$) was assessed by integrating the outlet N concentration in the liquid (breakthrough curve):

$$m_{N,sorbed,BP} = Q \cdot \int_0^{t_{BP}} \left(C_{N,IN} - C_{N,OUT}\right) \cdot dt \qquad (3)$$

where Q indicates the volumetric flow rate and t_{BP} the time corresponding to the selected BP.
The desorption/regeneration procedure was performed by counter-current elution of 2 BVs of deionized (DI) water to wash the TMWW from the adsorption bed and, then, 10 BVs of a KCl or KNO_3 solution (50 g L^{-1} in the natural zeolite tests and 10 g L^{-1} in the G13 tests) to regenerate the adsorbent and recover the N-rich product. Desorption was performed at a 20-minute EBCT, a commonly used contact time (Hedström, 2001). The number of BVs in the regeneration was chosen to ensure the complete desorption of all cations. The complete regeneration of the bed was verified by monitoring the outlet stream. More details about column packing, apparatuses and procedures for parameter determination from the breakthrough curves can be found in Pinelli et al., 2016 and 2022, and Frascari et al., 2019.

2.3 Characterization of granules

The morphological and macro-structural features of the granules were investigated by digital microscopy (3D Digital Microscope RH2000, Hirox, Japan).
The poured bulk density of the granules was determined by pouring the granules of known mass into a graduated cylinder and measuring the occupied volume. Tapped density was then determined by measuring the volume occupied by the granules after tapping the graduated cylinder. Densities were calculated as the ratio of the mass of the granules to the volume occupied by them.
The true density – i.e. mass/volume of the solid material - was obtained by helium pycnometer (Accupyc 1330, Micromeritics).
X-ray diffraction (XRD) patterns were collected using a Powder Diffractometer Bruker D8 Advance with CuKα radiation, Karlsruhe, Germany, on the powdered granules.
The elemental composition of the granules was determined by X-Ray Fluorescence (XRF) analysis on powdered material. Measurements were performed by X-MET7500 Mining Analyser (Oxford Instruments) equipped with Mining_LE_FP (standardless Fundamentl Parameter Calibration).
Possible modifications in the geopolymer vibrating mode after adsorption test were evaluated by Attenuated Total Reflection (ATR) measurements obtained using a Thermo Scientific Nicolet iS5 FTIR Spectrometer equipped with an iD7 ATR accessory and diamond crystal. Each spectrum was accumulated from 32 individual measurements, in the acquisition range 4000-400 cm^{-1}, performed on pulverized granules.

Pore size distribution, in the range 0.0058–100 µm, was analyzed by mercury intrusion porosimetry, MIP (Thermo Finnigan Pascal 140 and Thermo Finnigan Pascal 240), with an instrument accuracy of 4%. Total porosity was roughly estimated using the bulk density calculated from MIP analysis (volume of the analysis cell occupied by granules) and true density obtained by helium pycnometer.
The measurement of the specific surface area (SSA) was carried out in a Thermo Scientific™ Surfer instrument. The specific surface area was calculated by the Brunauer–Emmett–Teller (BET) method, by means of nitrogen adsorption at 77 K.
Mechanical tests were performed simultaneously on several granules (≈0.8 g of granules for each test), at room temperature as reported in Papa et al. (2021) according to the international standard ISO 18591. The applied standard allows to calculate the average compressive strength of the granules (Pc) and the relative density of the compressed granules (ρc), in function of the applied pressure and performing the test at least 4 times.

3. Results and Discussion

3.1 Ammonium adsorption/regeneration tests

The performance of G13 was compared to that of the natural zeolite activated in K^+ form. The comparison was based on batch equilibrium tests (isotherms) with an actual TMWW and in a pilot plant continuous flow tests, designed for testing adsorbents with an adsorption bed like those used in ion exchange process at full scale.

3.1.1 Isotherm tests

The first step of the comparison was to run an isotherm with the actual TMWW (Table 1), spiked with different amounts of NH_4Cl. The experimental data and the best fitting interpolations conducted with the Langmuir model are shown in Fig. 1. The scrutiny of Fig. 1 suggests similar equilibrium adsorption performances with a favorable isotherm type for both G13 and the natural zeolite. In order to have an estimation of the ammonium sorption performances in the actual operating conditions, the Langmuir model was used to interpolate the isotherm experimental data and the best-fitting parameters were used to estimate the operating capacity in equilibrium with an ammonium concentration of 40 $mg_N\ L^{-1}$, the typical value expected in a TMWW with no nitrogen removal. The value obtained with G13 was 9.3±1.7 $mg_N\ g^{-1}$, 27% higher than that of the natural zeolite (7.3±1.5 $mg_N\ g^{-1}$ of dry adsorbent). This result is a first indication that G13 is potentially a better adsorbent than the natural zeolite, also in the presence of competing cations.
A rough estimation of the cation exchange capacity (CEC) of each material is the maximum adsorption capacity that can be obtained from the asymptotic value of the adsorbed concentration in the solid estimated by the best fit with Langmuir isotherm. The two values (36±15 $mg_N\ g^{-1}$ of dry adsorbent for G13 and 38±11 $mg_N\ g^{-1}$ for the natural zeolite) resulted similar and in good agreement with the CECs measured by means of the column method described in section 2.2.2, equal to 42±8 $mg_N\ g^{-1}$ for G13 and 34±3 $mg_N\ g^{-1}$ for the natural zeolite. It should be noted that the distance between the G13 and the Chabazite values decreases as the concentration in the liquid increases: the G13 isotherm is more favourable than the Chabazite isotherm, and the gain in the performance of G13 is higher at the low N concentrations targeted by the process of N recovery from MWW.

3.1.2 Continuous flow breakthrough tests

The concentrations of the main cations in the column outlet at different bed volumes (breakthrough curves) obtained with G13 and the natural zeolite are shown in Fig. 2 a and b respectively. In both cases, ammonium is the last cation eluted, confirming the good selectivity of both materials towards NH_4^+. However, the elution order is slightly different: Na^+, Mg^{2+}, Ca^{2+}, NH_4^+ for G13 and Mg^{2+}, Na^+, Ca^{2+}, NH_4^+ for natural zeolite. The elution of Na^+ before Mg^{2+} in the case of G13 is of interest in view of a potential reuse of the recovered product as a fertilizer. Indeed, the Na^+, Mg^{2+}, Ca^{2+}, NH_4^+ elution order allows to perform a fractionated desorption and the consequent collection of a fraction with a

very low concentration of Na^+, harmful for several crops. A description of the fractioned desorption is given later on in this section.
The high selectivity of the adsorbents towards NH_4^+ can be explained with the steric hindrance that cations encounter during diffusion inside the pores. In general, the greater the Al content of zeolites (i.e. the more extra framework cations needed to balance the charge), the higher the cation exchange capacity of the zeolite (Mumpton, 1999). As regards the selectivity and the sorption capacity of the zeolite for different cations, these are defined also by zeolite porosity, pore size distribution and specific surface area. Furthermore, natural zeolites from different deposits may vary widely in purity, chemical composition, crystal size, porosity, pore diameter and other properties, determining their sorption and ion exchange capacity (Wang and Peng, 2010). Therefore, the high selectivity in zeolites is mainly given by the particular microporous rigid structure, which can preferentially adsorb and accommodate different cations.
Since geopolymers are considered as the amorphous counterpart of zeolites, also their cation exchange capacity depends on the cations available for exchange, and at the same time, on the particular porosity developed during their synthesis. In both adsorbents, ammonium ions probably diffused easily in the interstices, whilst other cations as Na^+ were impeded by the bigger hydrate shell and were thus incorporated more slowly. Ammonium possesses a small hydrated radius, equal to about 0.15 nm (Sidey, 2016), smaller than the typical size of the channels and nanopores that are respectively in natural zeolite (0.37-0.42 nm for Chabazite, 0.28-0.48 nm for Phillipsite; Shoumkova, 2011) and in G13 (Landi et al., 2013). Conversely, the radiuses of the other hydrated cations are bigger (Israelachvili, 2011), comparable to the size of the natural zeolite microchannels, indicating that the exchange of these cations is likely to be limited by steric hindrance. Indeed, the determining factor is the hydration energy: smaller ions have a higher electric charge; therefore, they hydrate more easily and have a lower affinity for the exchanger, explaining the elution order.
A second important aspect of comparison between the two adsorbents is their capacity and in particular the ammonium operating capacity, that is the ammonium concentration that can be obtained in the adsorbent at the selected breakpoint in tests conducted in the presence of competing cations: this performance parameter is influenced not only by the total cation capacity, but also by the concentration in the TMWW and by the adsorbent selectivity. The expected effect of a higher operating capacity is a delayed breakpoint (namely an increase of the number of BVs necessary to reach the concentration limit) and this in turn reduces the treatment cost.
The number of BVs of treated TMWW and the operating capacity of G13 at the selected breakpoint, equal to 149 and 8.5 $mg_N\ g^{-1}$ of dry adsorbent, resulted 72% and 67% higher than the corresponding values obtained with the natural zeolite (87 BVs, operating capacity 5.1 $mg_N\ g^{-1}$). These operating capacities, assessed in continuous flow conditions, are lower than those estimated by means of the isotherm tests (9.3 $mg_N\ g^{-1}$ for G13, 7.3 $mg_N\ g^{-1}$ for the natural zeolite), since in continuous flow tests the adsorbent does not reach equilibrium in the whole bed. Nevertheless, they confirm a significantly better performance of G13 with respect to the tested natural zeolite. The adsorption yields were similar (97% for G13, 99% for the natural zeolite).
A final important aspect to be investigated is the possibility to easily regenerate the adsorbent after each adsorption phase and recover a N-rich desorbed product. The adsorption columns were regenerated with KCl in the first BT test, then a KNO_3 solution was used to obtain a desorbed product rich in NH_4NO_3, a widespread fertilizer. No differences were observed in the tests performed with Cl^- or NO_3^- as anions. The concentrations of desorbed ammonium in the regenerant versus the number of BVs of the regenerant fed are shown in Fig. 3 (a) and (b). Since G13 adsorbs cations more strongly than zeolite, the desorption process was quite slow, requiring 15 regenerant BVs to release 95% of the adsorbed N, versus 4 BVs needed using the natural zeolite. Nevertheless, the slow desorption of G13 highlights an important and positive feature of this material. Indeed, Fig. 3b clearly shows that it is possible to separate a first desorbed fraction (5 BVs) containing almost all the Na, and then collect separately a second fraction (6-16 BVs) containing 91% of the total desorbed ammonium. The mean N concentration in the second fraction was 0.75 $g_N\ L^{-1}$, a value 19 times higher than the initial N

content of the MWW (0.040 g_N L^{-1}) and that can be increased by further optimizing the desorption procedure. Indeed, optimal desorption conditions can be identified by means of a trade-off between the positive effect of the selective recover of ammonium with respect to sodium, and the higher operational cost associated to the larger amount of regenerant needed. The important result of this procedure is that the 2nd desorption fraction, the actual product, had a very low content of Na (0.022 g L^{-1}), a cation that should be minimized in fertilizers as it is harmful for several crops and for soil texture. The concentrations in the desorbed liquid were multiplied by the desorbed volume to calculate the mass of cations contained in the product, expressed as the mass of the corresponding salts. The 2nd desorption fraction obtained from the test regenerated with KNO_3 was mainly made of KNO_3 (56%$_{wt}$) and NH_4NO_3 (37%$_{wt}$), with a very low content in $NaNO_3$, just 0.06%$_{wt}$, the remaining 7%$_{wt}$ being composed by other nitrates. Indeed, the composition of the solid that can be obtained from the desorption solution is of vital importance in view of the reuse of the recovered product as a fertilizer. The results showed that, even without any further treatment, the desorbed product obtained in this work had a high ammonium content and a very low sodium content. Therefore, the combined effect of the very promising performance of G13 in terms of capacity and selectivity and the possibility that G13 allows to fraction the desorption product make G13 a very promising material for the optimization and scale-up of the ammonium removal & recovery process, leading to a final product that can potentially be used as an ammonium–rich nitrate-based fertilizer.
Due to a short-range order of the structure (Duxon et al., 2007), the amorphous nature of the mesoporous geopolymer affects the selectivity, being the ion paths more tortuous than in a crystalline zeolite. It follows that G13 differentiates cations better than the natural zeolite, on the basis of the steric hindrance, but the adsorption and desorption processes resulted slowed down.

3.2 Characterization of the adsorbent granules

In addition to a high adsorption capacity and selectivity, durability, robustness and easiness of regeneration are key features of a successful adsorbent. Therefore, G13 granules were characterized after seven adsorption/regeneration cycles (G13AR) and compared to G13 and fresh natural zeolite in order to assess possible changes or degradation effects on the material.

3.2.1 Morphological, chemical and textural characteristics

The optical microscope pictures in Fig. 4 show as-prepared natural zeolite, G13 and G13AR granules. Although the same crushing and sieving procedure was used, granules look very different. Zeolite granules have rounded edges with surface debris from softer phases (Fig. 4b). In fact, natural zeolites are not homogenous in composition as they belong to a mineral deposit of volcanic origin. Differently, G13 granules, being a synthetized product, are uniform with sharp edges (Fig. 4c) and clean fracture surfaces (Fig. 4d), typical of a material with a brittle fracture behavior. Notably, after the adsorption/regeneration cycles (Fig. 4e, f) neither size nor shape changed, the sharp edges were maintained and the surfaces remained integer (no cracks formation) preserving the rounded ultra-macropores formed by entrapped air in the geopolymer slurry during casting (Fig. 4d, f).
Fig. 5a shows the XRD pattern of the G13 geopolymer before and after the adsorption/regeneration cycles, showing no evidence of new phases in G13AR together with the typical amorphous hump centred around 27° 2θ (Duxson et al., 2007; Provis et al., 2005), and only few crystalline phases, such as quartz (#46-1045) and muscovite (#34-0175), belonging to the starting metakaolin (Papa et al., 2014). Moreover, ATR-FTIR spectra (Fig. 5b) of G13 and G13AR almost overlap, being the most significant bands, typical of geopolymers (Papa et al., 2022), superimposable also after adsorption/regeneration cycles, highlighting no modifications nor formation of new bonding signals in G13AR.
Table 2 reports the Si/Al and K/Al molar ratios: zeolite has a higher Si/Al ratio (2.6) than G13 (1.9), while K/Al ratio (0.6) is half that of the geopolymer. Zeolite also contains Ca^{2+} with a Ca/Al = 0.3. It should be noted that the Si/Al and K/Al ratios are calculated on the total quantity of elements present in the natural zeolite, i.e. belonging to all the other minerals not taking part to the adsorption process

in addition to chabazite and phillipsite, which have respectively Si/Al = 2 and Si/Al = 2.2 (Shoumkova, 2011) similarly to G13. In G13AR Si/Al and K/Al ratios did not statistically change, with values fixed on the theoretical ones, in particular regarding electroneutrality of K/Al = 1 (Davidovits, 2008) being K^+ the exchanged cation.
The poured and tapped true density, specific surface area (SSA) and the main values obtained by mercury intrusion porosimetry (MIP) are also reported in Table 2. Poured and tapped densities were higher for zeolite, since these are related to granules shape and size. Instead, true density was similar in G13 and natural zeolite, but it slightly decreased in G13AR, especially in terms of standard deviation as all the traces of unreacted potassium silicate were eliminated during repeated adsorption and regeneration cycles.
Regarding porosity, G13 and G13AR granules showed a total porosity of 50% and zeolite granules showed a value of 54%. Conversely, concerning MIP data in the range 0.0058-100 μm, G13 granules showed an open porosity and a total pore volume higher than natural zeolite ones (43% and 363 mm^3 g^{-1} compared to 30% and 259 mm^3 g^{-1}, respectively) and they remained about constant in G13AR. Furthermore, the pore size distributions were very different (Fig. 6): for natural zeolite granules porosity was broadly distributed along the dimensional acquisition range with the average pore size diameter of 0.12 μm, an order of magnitude smaller than the modal one (1.24 μm), the most frequent pore size diameter. Conversely, G13 and G13AR pore size distributions were monomodal, with the average and the modal pore size diameter centered at 0.01 μm for G13, and at a slightly higher value for G13AR (0.03 μm). Both distributions showed pores in the range of 10-100 μm, in accordance with the ultra-macropores revealed on the fracture surfaces of the geopolymer granules (Fig. 4). The assessment of the porosity in this range highlighted for both geopolymer and natural zeolite the presence of interconnected meso- and macropores, a crucial aspect to enable a fast mass transport and diffusion of cations towards the internal micropores (Chen et al., 2016). Furthermore, the pore diameter is one of the most important features of adsorbent materials that would affect the adsorbent selectivity based on the diameter of the adsorbed material (Kumar et al., 2012). The geopolymer selectivity is guarantee as the synthesis of the geopolymer is reproducible, i.e. the final synthetic product maintains the same characteristics (full geopolymerization, porosity, Si/Al ratio etc. However, it is important to point out that the measurement does not include the natural zeolite's microporosity, which is typically in the range of 0.37-0.42 nm for Chabazite and 0.28-0.48 nm for Phillipsite (Shoumkova, 2011). Conversely, G13 is predominantly mesoporous with the majority of smallest pores in the range of 20-40 nm (Landi et al., 2013). Finally, the specific surface area of natural zeolite is slightly higher than that of the geopolymer (Table 2), while it decreases from 77 m^2 g^{-1} in fresh G13 to 51 m^2 g^{-1} in G13AR.

3.2.2 Mechanical characterization

The robustness of the G13AR granules after the adsorption/regeneration cycles was investigated through the compaction of a bed of granules (ISO 18591 standard) and compared with the strength of the as-prepared G13 and natural zeolite granules. The mechanical durability of granules gives information on how much stresses the material can withstand during use (Antonyuk et al., 2005). The average compressive strengths (Pc) and density values (ρc) of the compacted granules are reported in Table 2. Fig. 7 shows the relative density versus the logarithmic pressure diagram used for calculating the strength of the granules. Indeed, the compressive strength was measured by locating the spot where the curve has the steepest curvature, at the intercept of the two regression lines showed, as an example, in Fig. 7 (Järveläinen et al., 2016). The granules are first packed and rearranged in the die: in fact, the initial relative density is equal to the poured density measured for the granules (Table 2). Subsequently, the point where relative density increases most rapidly while pressure increase is minimal is interpreted as the point of fracture of the granules (Järveläinen et al., 2016).
The compressive strength of as-prepared G13 granules resulted higher than that of natural zeolite. Furthermore, the adsorption/regeneration cycles determined a marked increase in G13AR compressive strength and a decrease in experimental error, demonstrating an improvement in

mechanical performance. The bed strength represents the overall strength of an average granule; the result is affected by the possible irregular force distribution in the bed, but in particular by size, porosity, and roughness of the granules (Antonyuk et al., 2005) together with the granules shape and internal imperfections (Subero-Couroyer et al., 2003). In bed compression, the result is also affected by the size distribution of the granules and by the friction among them (Kwan et al., 2015; Järveläinen et al., 2016). The granules are very different, as shown in Fig. 4. The presence of sharp edges in G13 granules avoided a high particle packing, therefore a higher pressure is required before failure occurs, increasing the compressive strength values. Moreover, granules strength can be affected by loading through a fatigue effect where a force below the granules' strength may cause further hardening, increasing the strength (Antonyuk et al., 2010), as possibly in the case of G13AR after adsorption/ regeneration cycles.

4. Conclusions

In view of a large-scale use as a fertilizer of the recovered ammonium from wastewaters, a metakaolin K-based geopolymer (G13) was compared to a natural zeolite composed of chabazite and phillipsite and activated in K^+ form, in terms of granules characterization and ammonium adsorption capacity. An actual treated municipal wastewater was used in the tests, conducted following a procedure that integrates batch isotherm tests and continuous-flow adsorption/desorption tests.

Despite a lower specific surface area, the G13 geopolymer resulted in a higher porosity and compressive strength in comparison with the natural zeolite. The ammonium removal tests indicated significantly better performances of G13 in terms of selectivity towards ammonium, operating capacity (8.5 mg_N g^{-1} of dry adsorbent), bed volumes of wastewater treated at the selected breakpoint (149) and possibility to obtain a fractionated desorbed product composed mainly by KNO_3 (56%$_{wt}$) and NH_4NO_3 (37%$_{wt}$), with a negligible concentration of Na (0.022 g L^{-1}), harmful for several crops. This product can potentially be used as a fertilizer in a circular economy perspective. Finally, the geopolymer granules did not deteriorate in their mechanical, morphological nor textural properties after repeated adsorption/regeneration cycles, highlighting the robustness of the selected material.

Overall, G13 resulted a very promising material for the optimization and scale-up of the ammonium recovery process.

Acknowledgements

The authors acknowledge the Partnership on Research and Innovation in the Mediterranean Area (PRIMA) Programme for funding the FIT4REUSE project under grant agreement number 1823 (https://fit4reuse.org/). The PRIMA Programme is supported under Horizon 2020, the European Union's Framework Programme for Research and Innovation. The authors greatly thank Ms. Maria Chiara Marchioni for sample preparation, Mr. Cesare Melandri for mechanical tests, Dr. Sabrina Gualtieri for XRF analysis and Golrokh Vatanishahmirzadi, Andrea Verdicchio and Carlo Filiani for cation analysis and test preparation.

References

Antonyuk, S., Heinrich, S., Tomas, J., Deen, N.G., Van Buijtenen, M.S., Kuipers, J.A.M., 2010. Energy absorption during compression and impact of dry elastic-plastic spherical granules. Granular Matter 12, 15-47.

Antonyuk, S., Tomas, J., Heinrich, S., Mörl, L., 2005. Breakage behaviour of spherical granulates by compression. Chem. Eng. Sci. 60, 4031-4044.

Asim, N., Alghoul, M., Mohammad, M., Amin, M.H., Akhtaruzzaman, M., Amin, N., Sopian, K., 2019. Emerging sustainable solutions for depollution: Geopolymers. Constr. Build. Mater. 199, 540-548. https://doi.org/10.1016/j.conbuildmat.2018.12.043

Beckinghausen, A., Odlare, M., Thorin, E., Schwede, S., 2020. From removal to recovery: An evaluation of nitrogen recovery techniques from wastewater. Appl. Energy 263, 114616. https://doi.org/10.1016/j.apenergy.2020.114616

Bell, J.L., Driemeyer, P.E., Kriven, W.M., 2009. Formation of ceramics from metakaolin-based geopolymers. Part II: K-based geopolymer. J. Am. Ceram. Soc. 92(3), 607–15. https://doi.org/10.1111/j.1551-2916.2008.02922.x
Bortnovsky, O., Dedecek, J., Tvaruzkova, Z., Sobalík, Z., Subrt, J., 2008. Metal ions as probes for characterization of geopolymer materials. J. Am. Ceram. Soc. 91, 3052-3057. https://doi.org/10.1111/j.1551-2916.2008.02577.x
Carrera, J., Baeza, J.A., Vicent, T., Lafuente, J., 2003. Biological nitrogen removal of high-strength ammonium industrial wastewater with two-sludge system. Water Res. 37, 4211–4221. https://doi.org/10.1016/S0043-1354(03)00338-5
Chen, D., Wang, L., Ma, Y., Yang, W., 2016. Super-adsorbent material based on functional polymer particles with a multilevel porous structure. NPG Asia Mater. 8, e301. doi: 10.1038/am.2016.117.
Chen, H.-F., Lin, Y.-J., Chen, B.-H., Yoshiyuki, I., Liou, S. Y.-H., Huang, R.-T., 2018. A further investigation of NH_4^+ removal mechanisms by using natural and synthetic zeolites in different concentrations and temperatures, Minerals 8, 499. https://doi.org/10.3390/min8110499
Davidovits, J., 2008. Geopolymers Chemistry and Applications, Institut Geopolymere, Saint-Quentin, France.
Duxson, P., Fernández-Jiménez, A., Provis, J.L., Lukey, G.C., Palomo A., van Deventer, J.S.J., 2007. Geopolymer technology: the current state of the art. J. Mater. Sci. 42, 2917–2933. https://doi.org/10.1007/s10853-006-0637-z
El-Eswed, B.I., 2019. Aluminosilicate inorganic polymers (geopolymers): emerging ion exchangers for removal of metal ions, in: Inamuddin, M. Ahamed, A. Asiri (Eds.), Applications of ion exchange materials in the environment. Springer Nature Switzerland AG, pp. 65-94. https://doi.org/10.1007/978-3-030-10430-6_4
Foglia, A., Akyol, Ç., Frison, N., Katsou, E., Eusebi, A. L., Fatone, F., 2020. Long-term operation of a pilot-scale anaerobic membrane bioreactor (AnMBR) treating high salinity low loaded municipal wastewater in real environment. Sep. Purif. Technol. 236, 116279. https://doi.org/ 10.1016/j.seppur.2019.116279.
Franchin, G., Pesonen, J., Luukkonen, T., Bai, C., Scanferla, P., Botti, R., Carturan, S., Innocentini, M., Colombo, P., 2020. Removal of ammonium from wastewater with geopolymer sorbents fabricated via additive manufacturing. Mater. Des. 195, 109006. https://doi.org/10.1016/j.matdes.2020.109006
Frascari, D., Molina Bacca, A.E., Wardenaar, T., Oertlé, E., Pinelli, D., 2019. Continuous flow adsorption of phenolic compounds from olive mill wastewater with resin XAD16N: life cycle assessment, cost–benefit analysis and process optimization. J. Chem. Technol. Biotechnol. 94, 1968-1981. DOI: 10.1002/jctb.5980.
Ge, Y., Cui, X., Kong, Y., Li, Z., He, Y., Zhou, Q., 2015. Porous geopolymeric spheres for removal of Cu(II) from aqueous solution: synthesis and evaluation. J. Hazard. Mater. 283, 244–25.
Guida, S., Potter, C., Jeferson1, B., Soares, A., 2020. Preparation and evaluation of zeolites for ammonium removal from municipal wastewater through ion exchange process. Sci. Rep. 10, 12426. https://doi.org/10.1038/s41598-020-69348-6
Hedström, A., 2001. Ion exchange of ammonium in zeolites: a literature review. J. Environ. Eng. 127, 673–681.
Huang, X., Guida, S., Jefferson, B., Soares, A., 2020. Economic evaluation of ion-exchange processes for nutrient removal and recovery from municipal wastewater. Clean Water 3, 7. https://doi.org/10.1038/s41545-020-0054-x
Israelachvili, J. N., 2011. Interactions Involving Polar Molecules, in Intermolecular and Surface Forces, Elsevier, 71–90. doi: 10.1016/b978-0-12-375182-9.10004-1.
Järveläinen, M., Kaleva, A., Kaitajärvi, A., Laakso, J., Kanerva, U., Levänen, E., 2016. Compression curve analysis and compressive strength measurement of brittle granule beds in lieu of individual granule measurements. Particuology 29, 60-68. https://doi.org/10.1016/j.partic.2015.10.006.

Jha, V.K., Hayashi, S., 2009. Modification on natural clinoptilolite zeolite for its NH_4^+ retention capacity. J. Hazard. Mater. 169, 29–35. https://doi.org/10.1016/j.jhazmat.2009.03.052
Kumar, P., Agnihotri, R., Wasewar, K.L., Uslu, H., Yoo C., 2012. Status of adsorptive removal of dye from textile industry effluent. Desalin. Water Treat. 50, 226–244. https://doi.org/10.1080/19443994.2012.719472.
Kwan, A.K.H., Wong, V., Fung, W.W.S., 2015. A 3-parameter packing density model for angular rock aggregate particles. Powder Technol. 274, 154-162.
Landi, E., Medri, V., Papa, E., Dedecek, J., Klein, P., Benito, P., Vaccari, A., 2013. Alkali-bonded ceramics with hierarchical tailored porosity. Appl. Clay Sci. 73, 56–64.
Luukkonen, T., Heponiemi, A., Runtti, H., Pesonen, J., Yliniemi, J., Lassi, U., 2019. Application of alkali-activated materials for water and wastewater treatment: a review. Rev. Environ. Sci. Biotechnol. 18, 271-297. https://doi.org/10.1007/s11157-019-09494-0
Luukkonen, T., Věžníková, K., Tolonen, E.-T., Runtti, H., Yliniemi, J., Hu, T., Kemppainen, K., Lassi, U., 2018. Removal of ammonium from municipal wastewater with powdered and granulated metakaolin geopolymer. Environ. Technol. 39(4), 414-423. https://doi.org/10.1080/09593330.2017.1301572
Luukkonen, T., Tolonen, E.-T., Runtti, H., Kemppainen, K., Perämäki, P., Rämö, J., Lassi, U., 2017. Optimization of the metakaolin geopolymer preparation for maximized ammonium adsorption capacity. J. Mater. Sci. 52, 9363–9376. https://doi.org/10.1007/s10853-017-1156-9
McDowell, G.R., de Bono, J.P., 2013. On the micro mechanics of one-dimensional normal compression. Géotechnique 63, 895-908.
Medri, V., Papa, E., Mor, M., Vaccari, A., Natali Murri, A., Piotte, L., Melandri, C., Landi, E., 2020a. Mechanical strength and cationic dye adsorption ability of metakaolin-based geopolymer spheres. App. Clay Sci. 193, 105678. https://doi.org/10.1016/j.clay.2020.105678
Medri, V., Papa, E., Lizion, J., Landi, E., 2020b. Metakaolin-based geopolymer beads: Production methods and characterization. J. Clean. Prod. 244, 118844. https://doi.org/10.1016/j.jclepro.2019.118844
Medri, V., Papa, E., Dedecek, J., Jirlova, H., Benito, P., Vaccari, A., Landi, E., 2013. Effect of metallic Si addition on polymerization degree of in situ foamed alkali-aluminosilicates. Ceram. Int. 39, 7657-7668. https://doi.org/10.1016/j.ceramint.2013.02.104
Mumpton, F. A. 1999. La roca magica: Uses of natural zeolites in agriculture and industry. Proc. Natl. Acad. Sci. USA (Colloquium Paper) 96, 3463-3470.
Niu, X., Elakneswaran, Y., Islam, C.R., Provis, J.L, Sato, T., 2022. Adsorption behaviour of simulant radionuclide cations and anions in metakaolin-based geopolymer. J. Hazard. Mater. 429, 128373. https://doi.org/10.1016/j.jhazmat.2022.128373.
Novais, R.M., Seabra, M.P., Labrincha, J.A., 2017. Porous geopolymer spheres as novel pH buffering materials. J. Clean. Prod. 143, 1114-1122.
Papa, E., Landi, E., Miccio, F., Medri, V., 2022. K_2O-metakaolin-based geopolymer foams: production, porosity characterization and permeability test. Materials 15, 1008. https://doi.org/10.3390/ma1503100
Papa, E., Natali Murri, A., Vaccari, A., Landi, E., Medri, V., 2021. Geopolymer-hydrotalcite hybrid beads by ionotropic gelation. Appl. Clay Sci. 215, 106326.
Papa, E., Medri, V., Benito, P., Vaccari, A., Bugani, S., Jaroszewicz, J., Swieszkowski, W., Landi, E., 2015. Synthesis of porous hierarchical geopolymer monoliths by ice-templating, Micropor. Mesopor. Mater. 215, 206-214. https://doi.org/10.1016/j.micromeso.2015.05.043
Papa, E., Medri, V., Landi, E., Ballarin, B., Miccio, F., 2014. Production and characterization of geopolymers based on mixed compositions of metakaolin and coal ashes. Mater. Des. 56, 409-415. https://doi.org/10.1016/j.matdes.2013.11.054
Pinelli, D., Molina Bacca, A.E., Kaushik, A., Basu, S., Nocentini, M., Bertin, L., Frascari, D., 2016. Batch and Continuous Flow Adsorption of Phenolic Compounds from Olive Mill Wastewater: A

Comparison between Nonionic and Ion Exchange Resins. Int. J. Chem. Eng., 2016, 9349627. DOI: 10.1155/2016/9349627.
Pinelli, D., Bovina, S., Rubertelli, G., Martinelli, A., Guida, S., Soares, A., Frascari, D., 2022. Regeneration and modelling of a phosphorous removal and recovery hybrid ion exchange resin after long term operation with municipal wastewater. Chemosphere 286, 131581.
Provis, J.L., Lukey, G.C., van Deventer, J.S.J., 2005. Do geopolymers actually contain nanocrystalline zeolites?a reexamination of existing results. Chem. Mater. 17, 3075-3085.
Rasaki, S.A., Bingxue, Z., Guarecuco, R., Thomas, T., Minghui, Y., 2019. Geopolymer for use in heavy metals adsorption, and advanced oxidative processes: A critical review. J. Clean. Prod. 213, 42-58. https://doi.org/10.1016/j.jclepro.2018.12.145
Rohm and Hass Company, 2005. Laboratory Procedures for Testing Amberlyst™ and Amberlite™ ion exchange resins and adsorbents.
Sanguanpak, S., Wannagon, A., Saengam, C., Chiemchaisri, W., Chiemchaisri, C., 2021. Porous metakaolin-based geopolymer granules for removal of ammonium in aqueous solution and anaerobically pretreated piggery wastewater. J. Clean. Prod. 297, 126643. https://doi.org/10.1016/j.jclepro.2021.126643
Shoumkova, A., 2011. Zeolites for water and wastewater treatment: An overview," Research Bulletin of the Australian Institute of High Energetic Materials, Special Issue on Global Fresh Water Shortage, vol. 2, no. 10.
Sidey, V., 2016. On the effective ionic radii for ammonium. Acta Crystallogr. Sect. B: Struct. Sci. Cryst. Eng. Mater. 72, 626–633. doi: 10.1107/S2052520616008064.
Siyala, A.A., Shamsuddina, M.R., Khana, M.I., Rabata, N.E., Zulfiqara, M., Mana, Z., Siamec, J., Azizli, K.A., 2018. A review on geopolymers as emerging materials for the adsorption of heavy metals and dyes. J. Environ. Manage. 224, 327–339. https://doi.org/10.1016/j.jenvman.2018.07.046
Subero-Couroyer, C., Ghadiri, M., Brunard, N., Kolenda, F., 2003. Weibull analysis of quasi-static crushing strength of catalyst particles. Chem. Eng. Res. Des. 8, 953-962.
Tan, T. H., Moa, K. H., Ling, T.-C., Lai, S. H., 2020. Current development of geopolymer as alternative adsorbent for heavy metal removal. Environ. Technol. Innov. 18, 100684.
Tasić, Ž.Z., Bogdanović, G.D., Antonijević, M.M., 2019. Application of natural zeolite in wastewater treatment: A review. J. Min. Metall. A: Min. 55(1), 67-79. https://doi.org/10.5937/JMMA1901067T
Thornton, A. 2007. The application of Mesolite for ammonium removal from municipal wastewaters, Cranfield University, Bedford.
Wang, S., Peng, Y., 2010. Natural zeolites as effective adsorbents in water and wastewater treatment. Chem. Eng. J. 156, 11-24. https://doi.org/10.1016/j.cej.2009.10.029.

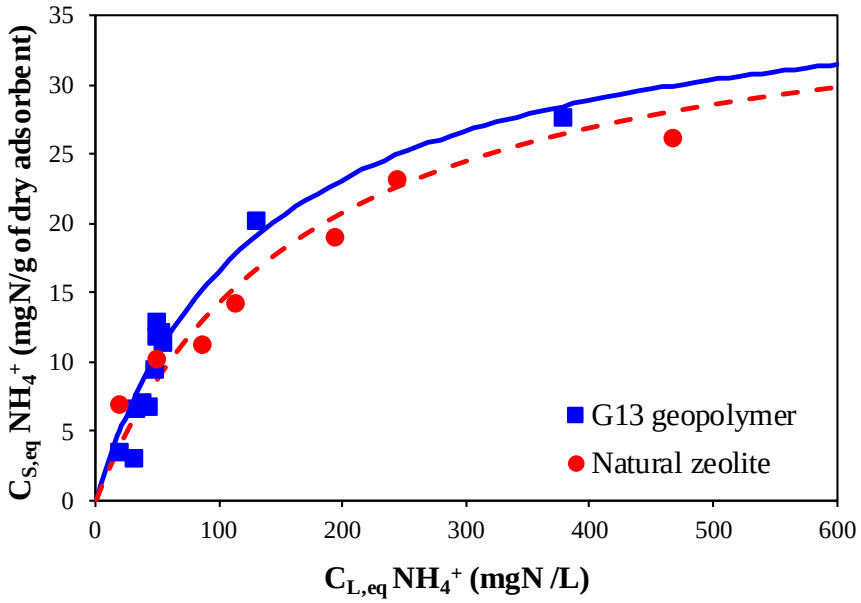

Figure 1. Isotherms conducted with G13 and natural zeolite in K^+ form and saline TMWW. Continuous and dashed lines represent best-fitting simulations obtained with the Langmuir model.

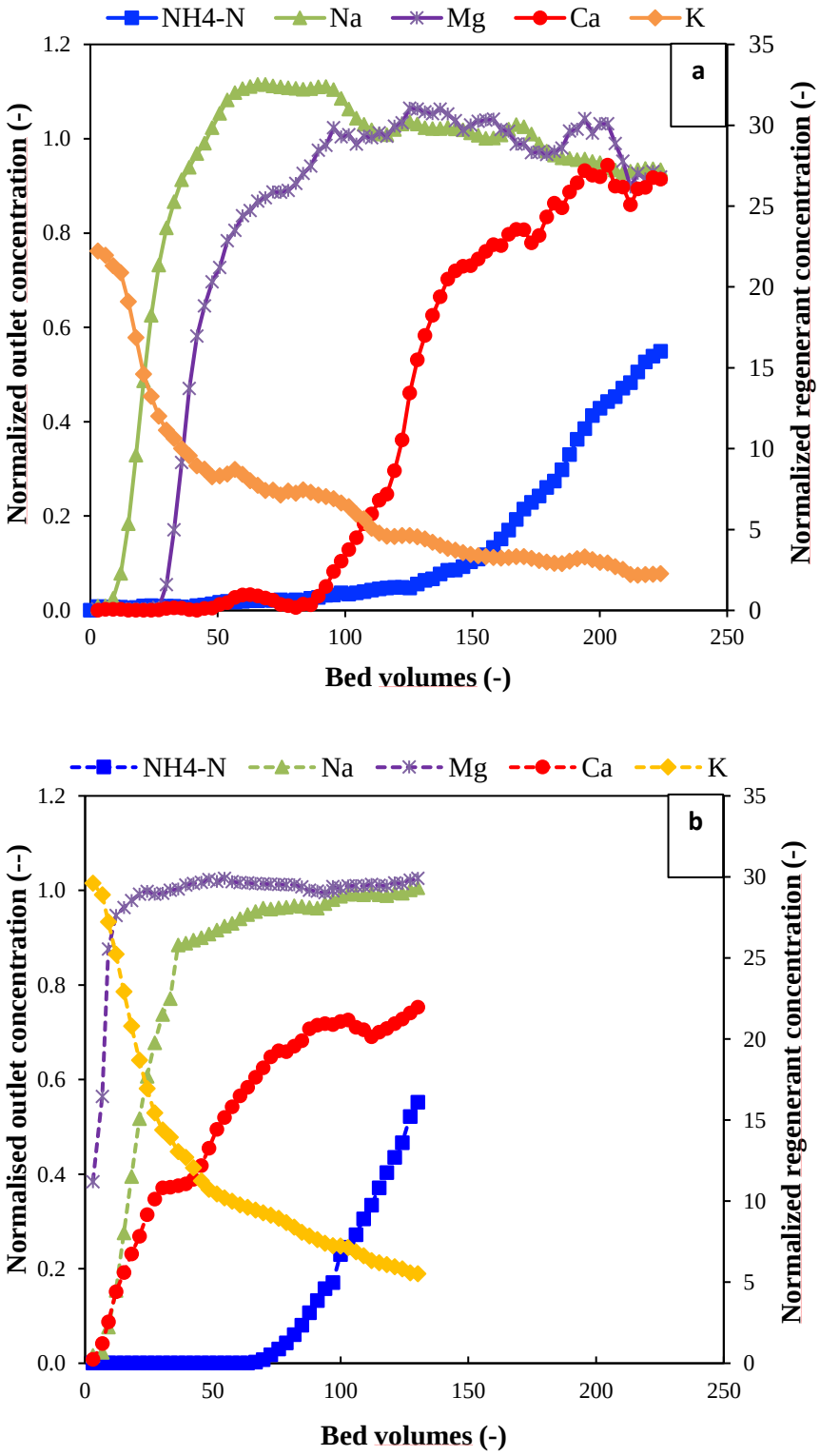

Figure 2. Breakthrough curves obtained with a) G13 and b) natural zeolite in K^+ form, in tests conducted with saline TMWW with an empty bed contact time (EBCT) of 10 min. The concentrations are normalised by the inlet concentrations in the MWW (40 mg_N L^{-1}, 214 mg_{Na} L^{-1}, 24 mg_K L^{-1}, 32 mg_{Mg} L^{-1}, 97 mg_{Ca} L^{-1}).

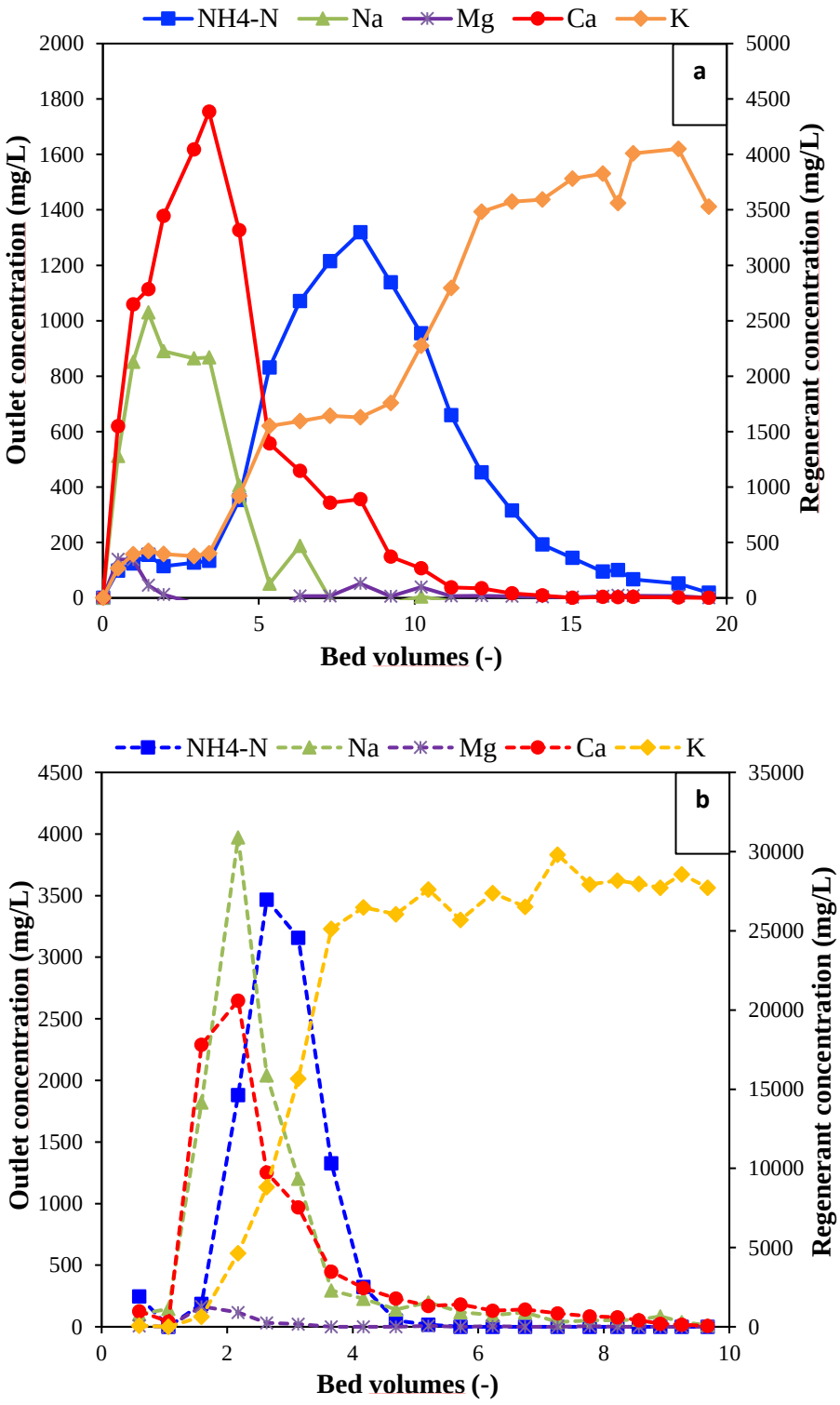

Figure 3. Desorption breakthrough curves obtained with a) G13 and b) natural zeolite in K^+ form, in regeneration tests conducted with a KCl solution.

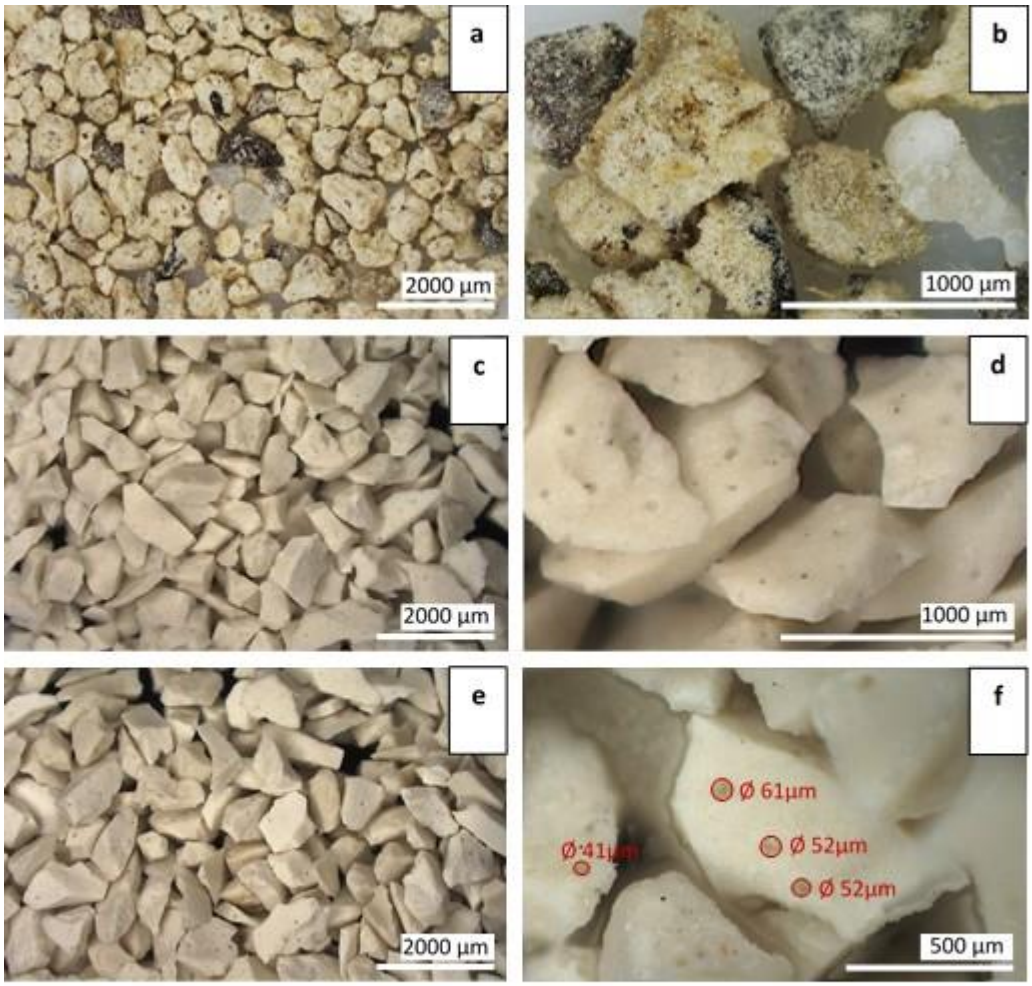

Figure 4. Digital microscope images of natural zeolite (a,b), G13 granules before (c,d) and after the adsorption/regeneration tests (G13AR) (e,f).

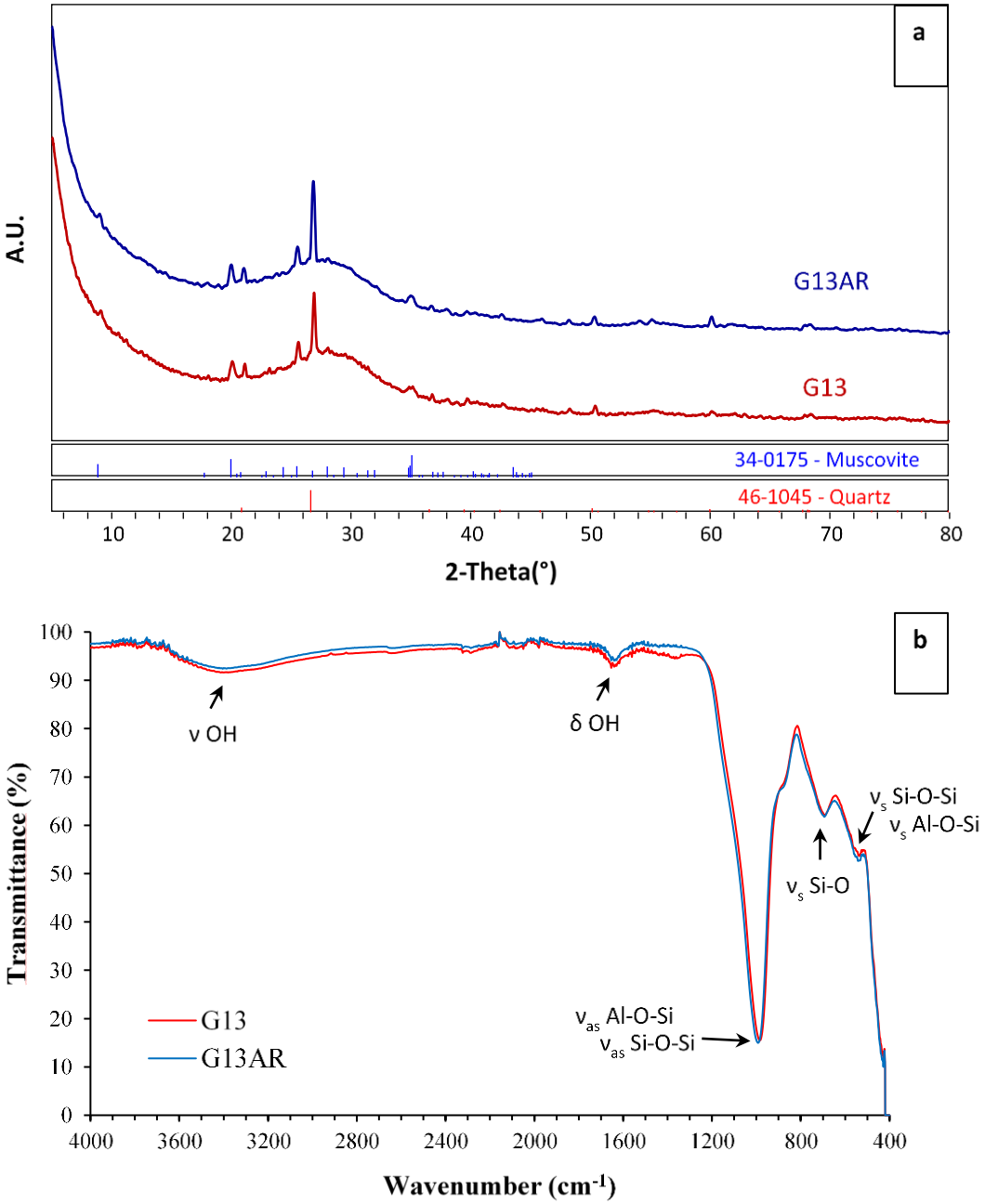

Figure 5. XRD patterns (a) and ATR-FTIR spectra (b) of geopolymer G13 and G13AR. ATR-FTIR spectra evidence the presence of the typical geopolymer bands: stretching (ν) and bending (δ) vibrations of OH groups, asymmetric stretching (vas) of Si–O–Si and Si–O–Al, Si-O symmetrically stretching (vs Si-O) and the symmetric stretching (vs) of Si–O–Si and Al–O–Si.

Table 1. Composition of the high-salinity TMWW effluent used for the isotherm and continuous flow tests.

Compound	Symbol	Unit	Average value ± 95% confidence interval
Ammonium nitrogen	NH_4-N	$mg_N\ L^{-1}$	17 ± 2[a]
Sodium	Na^+	$mg\ L^{-1}$	214 ± 7
Potassium	K^+	$mg\ L^{-1}$	24 ± 3
Magnesium	Mg^{2+}	$mg\ L^{-1}$	32 ± 1
Calcium	Ca^{2+}	$mg\ L^{-1}$	97 ± 9
Phosphate	PO_4-P	$mg_P\ L^{-1}$	2.3 ± 0.2
Chloride	Cl^-	$mg\ L^{-1}$	311 ± 3
Nitrate	NO_3^-	$mg_N\ L^{-1}$	2.5 ± 1
Sulphate	SO_4^{2-}	$mg\ L^{-1}$	45 ± 1
Biological oxygen demand	BOD_5	$mg_{O2}\ L^{-1}$	42 ± 1
Chemical oxygen demand	COD	$mg_{O2}\ L^{-1}$	38 ± 5
Total suspended solids	TSS	$mg\ L^{-1}$	0.010 ± 0.001
Density		$mg\ L^{-1}$	1.00 ± 0.002
pH	pH	-	7.9 ± 0.2

[a] Before conducting the tests, this effluent was spiked with NH_4Cl to achieve 40 $mg_N\ L^{-1}$.

Table 2. Natural zeolite and geopolymer G13 before and after adsorption/regeneration cycles (G13AR): Si/Al and K/Al molar ratios assessed by XRF, poured, tapped and true density, porosity data from MIP analyses, SSA values and compressive strength Pc and critical density ρc.

Sample code	Si/Al	K/Al	Pour density (g cm^{-3})	Tap density (g cm^{-3})	True density (g cm^{-3})	Open porosity (%)	Tot pore volume (mm^3 g^{-1})	Average pore Ø (μm)	Modal pore Ø (μm)	SSA (m^2 g^{-1})	Pc (MPa)	ρc (g cm^{-3})
Zeolite	2.6 ±0.2	0.6 ±0.1[a]	0.77 ±0.01	0.73 ±0.02	2.256 ±0.003	30	259	0.12	1.24	109	57.5 ± 4.1	0.99 ± 0.02
G13	1.9 ±0.2	1.2 ±0.1	0.68 ±0.01	0.61 ±0.01	2.273 ±0.025	43	363	0.01	0.01	77	64.0 ± 6.1	0.75 ± 0.01
G13AR	1.9 ±0.2	1.0 ±0.1	0.66 ±0.01	0.63 ±0.01	2.242 ±0.005	41	362	0.03	0.03	51	76.5 ± 3.7	0.719 ± 0.004

[a] Zeolite contains also Ca^{2+} with Ca/Al=0.3.